J. Fluid Mech. (1967), *vol.* 29, *part* 3, *pp.* 513–538
Printed in Great Britain

Large-amplitude unsteady flow in liquid-filled elastic tubes

By JOHN H. OLSEN AND ASCHER H. SHAPIRO
Department of Mechanical Engineering, Massachusetts Institute of Technology, Cambridge, Massachusetts

(Received 25 October 1966)

Unsteady, large-amplitude motion of a viscous liquid in a long elastic tube is investigated theoretically and experimentally, in the context of physiological problems of blood flow in the larger arteries. Based on the assumptions of long wavelength and longitudinal tethering, a quasi-one-dimensional model is adopted, in which the tube wall moves only radially, and in which only longitudinal pressure gradients and fluid accelerations are important. The effects of fluid viscosity are treated for both laminar and turbulent flow. The governing non-linear equations are solved analytically in closed form by a perturbation expansion in the amplitude parameter, and, for comparison, by numerical integration of the characteristic curves. The two types of solution are compared with each other and with experimental data. Non-linear effects due to large amplitude motion are found to be not as large as those found in similar problems in gas-dynamics and water waves.

Symbols

A internal tube area
C wave speed; $C^2 \equiv (A/\rho)(dP/dA)$
D internal tube diameter
F dimensionless wall friction, $\tau l/\rho A C_0^2$
G elastic constant
h tube wall thickness
i $\sqrt{-1}$
J_0, J_1 Bessel functions
l tube length
N reduced frequency, $\omega l/C_0$
P pressure difference across tube wall
Q instantaneous volume flow rate at any section
Q_0 amplitude of oscillatory component of Q at $x = 0$
R tube internal radius
Re Reynolds number based on maximum volume flow and on D_0;

$$Re \equiv 4Q_0(1+s)/\pi D_0 \nu$$

s ratio of steady volume flow to amplitude of oscillatory volume flow at $x = 0$

t time
v instantaneous mean longitudinal velocity at any cross-section
W hoop tensile force in tube wall per unit length
x length co-ordinate
X see (31) and (33)
Y see (31) and (33)
α unsteady flow Reynolds number, $(\omega R^2/\nu)^{\frac{1}{2}}$
ϵ amplitude parameter, Q_0/A_0C_0
λ wavelength
μ fluid viscosity
ν kinematic viscosity
ξ $X-iY$
ρ density of liquid
τ wall shear force per unit length of tube
ω circular frequency of motion
ζ normalized inverse area, A_0/A.

Subscripts

n denotes conditions with no pressure difference across tube wall
0 denotes conditions with tube inflated but no motion
1, 2 order of terms in perturbation solution.

1. Introduction

The object of this investigation is to develop a theory for large-amplitude, unsteady flows of a viscous incompressible liquid in a long elastic tube, and to test this theory by experiments designed for that purpose. Standing waves with harmonic excitation are chosen for the experiments because of the ease of accurately setting boundary conditions. However, the analytical methods developed are equally applicable to travelling waves or to any arbitrary boundary conditions at the tube ends.

The results are relevant to blood flow in the larger ducts of the human vascular system, as well as to other unsteady flow problems where the compliance of the liquid is negligible compared with that of the tube wall.

A one-dimensional model for the flow is developed based on the assumptions that (i) the wavelength is long compared with the diameter, (ii) the tube is constrained from longitudinal motions, (iii) the liquid is incompressible and Newtonian, and (iv) the tube material follows the stress–strain law given by kinetic theory for rubber.

2. Range of the investigation

Previous work

Waves in an elastic tube filled with an incompressible liquid can be excited in many ways, e.g. transversely, in torsion, in longitudinal stretch, and by bulging. For each type of wave there is a wave speed and a corresponding set of suitable boundary conditions.

A recent survey article by Rudinger (1966) summarizes the theoretical literature of the subject, gives some comparisons with experiments, and has an extensive bibliography. The theories fall into two classes: (i) small-amplitude, linear theories, with the non-linear inertial terms of the equation of motion absent, and with a laminar treatment of friction (Womersely 1957; Morgan & Kiely 1954); and (ii) non-linear theories, using numerical integrations of the characteristics, and with various *ad hoc* treatments of laminar and turbulent friction (Lambert 1958; Streeter, Keitzer & Bohr 1964).

In the linear laminar-flow theories of Womersley (1957) and Morgan & Kiely (1954) an axisymmetric motion is treated, with the tube free to bulge and to move longitudinally. Two wave speeds are found, but both Womersley and Morgan & Kiely ignore one wave speed and its related boundary conditions. When the boundary conditions for either pressure or flow at the ends of the tube are given, but only one speed is admitted, the necessary additional conditions on the longitudinal motion of the ends cannot be given. Consequently the theories of Womersley and of Morgan & Kiely predict an excess longitudinal motion that has not been observed.

Lambert (1958) treated the human aorta as a one-dimensional, non-linear, inviscid problem by numerical integration of the characteristics, but his results are unfortunately meaningless since he took the flow speed to be many times the wave speed, instead of vice versa, owing to the omission of the numerical factor $\sqrt{980}$ in the computation of wave speed.

Streeter *et al.* (1964) dealt with unsteady flow in the larger vessels of the arterial system of a dog by a one-dimensional numerical integration of the characteristics, using Poisseuille's law for laminar friction and the empirical relationship between friction coefficient and Reynolds number for steady turbulent pipe flow, and neglecting the phase lag between instantaneous volume flow and wall shear stress. The pressure-area relationship employed for the tube is in serious question on three counts: first, the use of a constant Hooke's modulus; second, neglect of the relationship between radial and longitudinal strains involving Poisson's ratio; and, third and most important, the assumption that the fractional changes in diameter are negligible compared with the fractional changes in pressure, an unwarranted assumption contradicted by the numerical results themselves.

In the present state of affairs, it would be useful (i) to develop a non-linear theory in closed form, at least to second-order terms, and to establish its range of validity by numerical experiments in which it is compared with numerical integrations of the characteristics, (ii) to incorporate in the theory more accurate representations of the wall friction, (iii) to employ as part of the theory a pressure-area relationship more representative of rubber-like materials and to establish the effects of this on non-linear behaviour, and (iv) to perform related simple experiments designed not to simulate an animal arterial system, but rather to test the theoretical approximations and assumptions.

The present investigation attempts the foregoing objectives.

The motion to be considered

Arteries in the human vascular system are constrained longitudinally at points much closer than one wavelength apart. Hence longitudinal motions are negligible. We therefore assume that longitudinal displacements are zero and we limit the investigation to purely axisymmetric bulging modes, such as are caused by the injection of fluid at one end.

For small amplitudes a sinusoidal excitation at one end causes the tube to vibrate in a natural mode where motions at all points are sinusoidal functions of time. A harmonic excitation is therefore chosen for study because deviations from sinusoidal motion are then due to non-linear effects only and can be used as a simple test for non-linearity.

Parameter	Range for the larger human arteries	Range in present experiments
λ/R	Greater than 100	Greater than 1000
ϵ	0·18–0·01	0·19–0·007
α	17·0–3·0	25–1·9
Re	10,000–500	28,000–120
N	Not applicable	0·5–14·0
s	0·5–0·1	9·0–0
$P_0/\rho C_n^2$	0·28	0·2
h/R	0·1	0·13
D_0/D_n	—	1·2
D_n (cm)	1·0–5·0	0·635
ω (c/s)	0·5–3·0	0·07–2
μ (cp)	2·5–5·0	1–75
C_n (m/s)	5·0–10·0	11

TABLE 1

Parameters for the motion

Table 1 shows a comparison of the important parameters of the present experiments with physiological values for the larger arteries of the human vascular system. The physiological value for ω is taken as the circular frequency of the first harmonic of the heart output.

No attempt was made to model the anomalous viscosity of blood. The arteries were taken to be thin-walled elastic tubes whose mechanical properties are accounted for by the quantities C_0 and C_n.

3. The governing equations

Fluid dynamical conservation laws

Womersley (1957) has shown from order-of-magnitude arguments that when the wavelength λ is much greater than the tube radius R, the radial accelerations and pressure gradients are negligible. Noting from table 1 that λ/R is indeed very large, we consider a one-dimensional model in which only longitudinal fluid accelerations and forces are included. To simplify the problem further we ignore

the actual velocity profile except as it affects the wall friction, and we deal only with the mean velocity v parallel to the tube axis.

Observing that the cross-sectional area A depends on both position x and time t, and that the liquid is incompressible, we express the conservation of liquid volume by

$$\partial A/\partial t + \partial(vA)/\partial x = 0. \tag{1}$$

The one-dimensional momentum equation is

$$\frac{\partial P}{\partial x} + \rho\frac{\partial v}{\partial t} + \rho v\frac{\partial v}{\partial x} = -\frac{\tau}{A}, \tag{2}$$

in which the momentum flux at any section is approximated as $\rho A v^2$, which is exact only for a flat velocity profile. However, it has been shown by Olsen (1966) that this approximation produces a small error only in the non-linear terms. In an extreme case, namely Poiseuille flow, the true momentum flux is $\frac{4}{3}\rho A v^2$.

Since P is later assumed a function of A alone, we introduce the definition

$$C^2 \equiv (A/\rho)(dP/dA), \tag{3}$$

where C is later identified as the wave speed. Then, since

$$\partial P/\partial x = (dP/dA)(\partial A/\partial x) = (C^2\rho/A)(\partial A/\partial x),$$

equation (2) becomes

$$C^2\partial A/\partial x + A\,\partial v/\partial t + Av\,\partial v/\partial x = -\tau/\rho. \tag{4}$$

For the calculations of the relation between pressure and tube area, we may ignore longitudinal stresses in the tube wall as well as that part of the membrane force produced by longitudinal curvature, inasmuch as a large value of λ/R implies that both the longitudinal slope and the longitudinal curvature of the tube wall are small. Moreover, the density of the tube wall is of the same order as that of the liquid; therefore, we may neglect the radial inertia of the tube wall for the same reason that we neglected that of the liquid. With the foregoing assumptions, the simple statical equilibrium between hoop stress and excess internal pressure yields

$$W = PR.$$

Since the tube is longitudinally constrained, the relation between the hoop tension per unit length, W, and the extension ratio, R/R_n, is the same as that given by Treloar (1958) as

$$W = Gh_n[(R/R_n) - (R_n/R)^3], \tag{5}$$

where G is an elastic constant which is a property of the particular rubber used. Equation (5), derived from kinetic theory, has been shown experimentally (Treloar 1958) to be valid for both large and small deformations. Hence

$$P = (\tfrac{1}{2}\rho C_n^2)\,[1 - (A_n/A)^2], \tag{6}$$

where

$$C_n^2 \equiv 2Gh_n/\rho R_n, \tag{7}$$

from which, with (3),

$$C = C_n(A_n/A). \tag{8}$$

Nicholson (1966) has shown that the large-deformation stress-strain law of (5), (6), (7) and (8), in combination with the non-linear hydrodynamic terms, leads fortuitously to simpler end results than does a Hookean stress-strain law.†

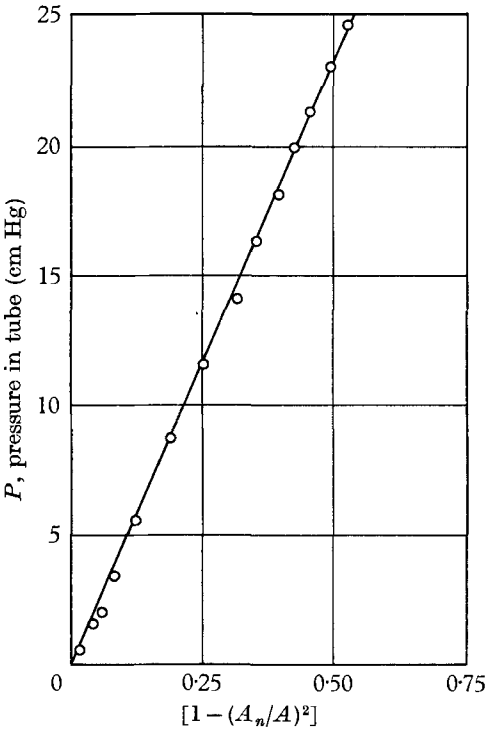

FIGURE 1. Experimental data for inflation pressure P *vs.* area A, plotted with the variables of (6). The straight line is the best fit to the data.

Experimentally derived properties

Equation (7) shows that the quantity ρC_n^2 contains all the static mechanical properties of the tube relevant to the wave propagation. Measurements of this quantity and of the liquid density ρ, therefore, establish the wave speed. Equation (6) shows that $\frac{1}{2}\rho C_n^2$ can be easily determined as the slope of a line of P *vs.* $[1-(A_n/A)^2]$. Figure 1 gives data from experiments in which the pressures P required to inflate the tube to different areas A were observed. That the data lie on a straight line shows that (6) is correct within the experimental range; the slope yields the value of C_n as 11·23 m/s.

Equation (6) is found experimentally to be valid only up to an area ratio A/A_n of about 2·5 (Nicholson 1966). Beyond this point, a three-dimensional state of

† The corresponding relations derived using Hooke's law with the conditions of zero longitudinal strain and Poisson's ratio of $\frac{1}{2}$ are (Olsen 1966):

$$P = 2\rho C_n^2[(A_n/A)^{\frac{1}{2}} - (A_n/A)],$$

$$C^2 = C_n^2[2(A_n/A) - (A_n/A)^{\frac{1}{2}}],$$

where $$C_n^2 \equiv Eh_n/2\rho R_n(1-\nu^2); \quad \nu = \tfrac{1}{2}.$$

Solutions corresponding to these are given by Olsen (1966).

strain can be found which, for the same tube volume, requires less internal pressure. The tube is unstable with respect to transition to this mode and large bulges appear on the tube. These bulges permanently deform the tube and ruin it for further experiments.

The above instability places a useful upper limit on the internal pressure in the tube. A useful lower limit also exists. If the pressure falls below the external pressure, the tube collapses unstably rather than remaining round, and no longer obeys (6). The collapse introduces very large non-linear effects not observed physiologically, and should be avoided experimentally through sufficient initial pressurization.

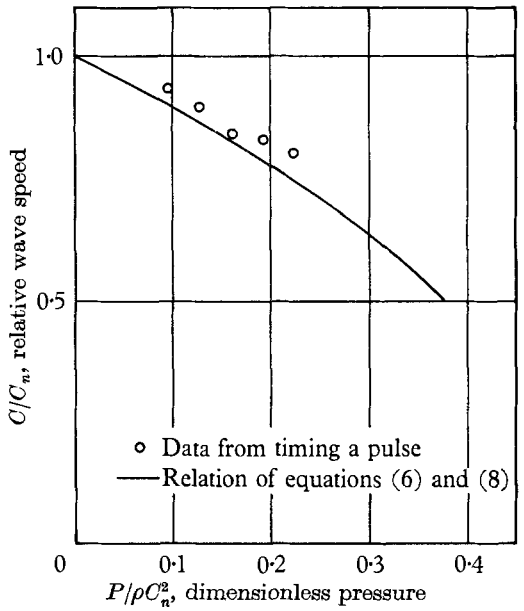

FIGURE 2. Experimental values of wave speed C for a small pulse, *vs.* inflation pressure P, compared (solid curve) with the value of C calculated from figure 1 and equations (6) and (8).

The solid curve of figure 2 shows C/C_n *vs.* $P/\rho C_n^2$ as calculated theoretically from (6) and (8). We shall show later that C is the speed of a small-amplitude wave in a frictionless fluid. The experimental points in figure 2 were determined, at different pressure levels P, by determining C_n under static conditions from the slope of the experimental line of figure 1, and by measuring C through timing the motion of a very small pressure pulse. The observed speeds, C, are slightly higher than those corresponding to the mechanical properties under static conditions. These differences are related to the time-dependent properties of the material.

The elastic constant G, which in figure 1 was determined statically, is in fact slightly dependent on the frequency. Figure 3 shows the relative force resulting from stretching a strip of rubber from the experimental tube at various frequencies of sinusoidal motion but at a fixed amplitude of about 50 % strain. The rubber appears stiffer at higher frequencies. In later comparisons with experimental results, C_n is therefore adjusted upward for higher frequencies, as follows: since

G is proportional to the relative force and C_n is proportional to $\sqrt{G}$, C_n as determined from figure 1 is corrected by multiplying the square root of the relative force of figure 3.

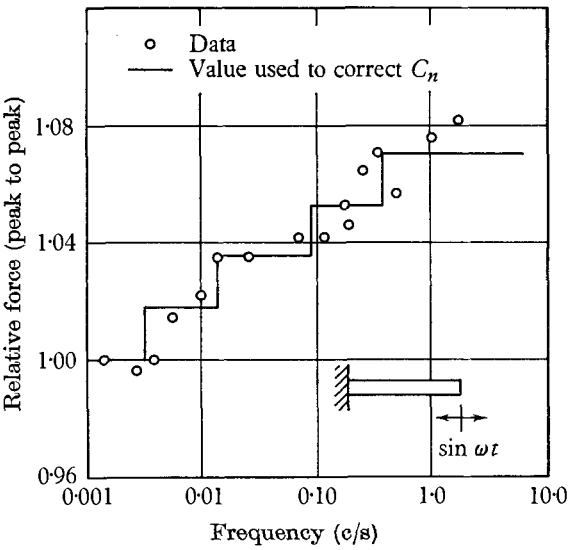

FIGURE 3. Effect of frequency on elastic stiffness of tube material.

The tube material showed negligible hysteresis effects but did exhibit a permanent strain of about 5% when stretched for the first time. After this initial set, it behaved like an elastic material except for the slight frequency dependence of G.

Approximation of the wall friction

The tube is very long, hence we neglect entrance effects near the ends of the tube. Since λ/R is very large, examination of the full continuity equation (including radial velocities) shows that the radial velocity is very much smaller than the longitudinal velocity. Therefore the longitudinal velocity profile at any section is virtually the same as if the tube were rigid. Consequently, the local shear force τ at the wall is assumed to be the same as in a rigid tube of the same diameter and having the same local conditions of flow history.

The exact relation for laminar flow in a rigid tube of constant area. With purely sinusoidal flow in a rigid tube, $Q = \mathrm{Im}\,(Q_0 e^{i\omega t})$, the exact solution (Womersley 1957; Schlichting 1960) for τ is

$$\tau = \mathrm{Im}\left[\frac{i\pi\mu\alpha^2}{A}(M_{10}^{-1}e^{-i\epsilon_{10}} - 1)Q\right],$$

where

$$M_{10}e^{i\epsilon_{10}} \equiv 1 - \frac{2J_1(\alpha i^{\frac{3}{2}})}{\alpha i^{\frac{3}{2}} J_0(\alpha i^{\frac{3}{2}})},$$

and

$$\alpha \equiv (\omega R^2/\nu)^{\frac{1}{2}}.$$

Thus, τ is linearly related to Q by a complex constant that is a function of α. Womersley (1957) has provided tables of the modulus, M_{10}, and of the argument, ϵ_{10}, for values of α from 0 to 10, as well as series expansions for α greater than 10.

With incompressible flow in a rigid tube of constant area, the problem is linear because the non-linear inertial terms in the equation of motion vanish. Thus a steady flow superposed on the oscillating flow requires that we simply add the Poiseuille shear force to that given above for oscillating flow. The Poiseuille shear force per unit length is $\tau = 8\pi\mu Q/A$ for a steady flow. Then, writing the total flow as $Q = Q_0(is + e^{i\omega t})$, where the physical flow is the imaginary part of this, the corresponding τ is

$$\tau = \mathrm{Im}\left\{\frac{iQ_0 s}{A}[8\pi\mu - i\pi\mu\alpha^2(M_{10}^{-1}e^{-i\epsilon_{10}} - 1)] + \frac{i\pi\mu\alpha^2 Q}{A}(M_{10}^{-1}e^{-i\epsilon_{10}} - 1)\right\}. \quad (9)$$

This relation is valid only for a sinusoidal flow with a steady component of arbitrary size. In a more general flow which is an arbitrary function of time the shear force depends not only on the instantaneous total flow, but also on the time history of the flow. The phase angle introduced by the complex constant relating τ and Q in (9) accounts completely for the time history dependence only in the sinusoidal case.

An approximate relation for laminar flow in a rigid tube. Numerical integration of the characteristics curves turns out to be much simplified if τ is linearly dependent only on the instantaneous value of the total flow, irrespective of the phase. This would be the case if $i\pi\mu\alpha^2(M_{10}^{-1}e^{-i\epsilon_{10}} - 1)$ were purely a real number. Making the approximation that τ and Q are related by only the real part of this constant, we get

$$\tau \cong \frac{Q_0 s}{A}\left(8\pi\mu - \pi\mu\alpha^2\frac{\sin\epsilon_{10}}{M_{10}}\right) + \frac{\pi\mu\alpha^2 Q}{A}\frac{\sin\epsilon_{10}}{M_{10}}, \quad (10)$$

where the imaginary part of (9) has already been taken so that τ and Q are the actual physical values. This approximation is used only in computational experiments where the perturbation solution is compared with the numerical integration of the characteristics. However, the approximation has some justification. First, we note that it affects only the unsteady portion of the flow. Later, with reference to figure 4, we note that the unsteady friction terms serve only to determine the values of two parameters X and Y as functions of α, where Y is related to the damping of the waves and X modifies the apparent wave speed. The approximation discussed here turns out to be accurate for high values of α and for very low values of α, and is at no point very poor.

The approximation for turbulent flow. The large Reynolds stresses in a turbulent flow cause the velocity profile to adjust to a change in flow more rapidly than it would in a laminar flow, and they also maintain a relatively flat velocity profile. As a heuristic approximation we assume that the adjustment time for a change in velocity profile is small compared to the period of the motion, which is equivalent to taking the flow as quasi-steady for the purpose of estimating turbulent friction.

For Reynolds numbers between 3000 and 30,000 the empirical friction data for a smooth pipe may be expressed as (Rohsenow & Choi 1961)

$$\frac{\tau/\pi D}{\frac{1}{2}\rho v^2} = \frac{0{\cdot}0791}{(vD/\nu)^{\frac{1}{4}}},$$

or

$$\tau = 0{\cdot}0396\pi\rho^{\frac{3}{4}}D^{\frac{3}{4}}\mu^{\frac{1}{4}}v^{\frac{7}{4}}[|v|/v]. \quad (11)$$

Use of the rigid tube results for the elastic tube. In applying the foregoing approximations for the wall friction, the diameter of the elastic tube is assumed not to change with x or t. This fixed diameter is taken at the state (subscript 0) for which the tube is at rest, but inflated to the volume about which the oscillations occur. This procedure introduces some error in the friction, but friction contributes only a small part of the total solution.

4. Theoretical solutions

The mathematical problem

The problem is to solve the set of equations (1), (4) and (8) with τ given by one of (9), (10) or (11).

With the experimental apparatus we can produce the combination of a steady throughflow $Q_0 s$ together with an unsteady flow which is sinusoidal at the inlet and which is made to vanish at the exit. The boundary conditions are therefore formulated as follows:

$$\text{at } x = 0: \quad Av = Q_0(s + \sin \omega t), \tag{12}$$

$$\text{at } x = l: \quad Av = Q_0 s. \tag{13}$$

Although the equations are hyperbolic, no initial conditions are necessary because we are seeking the ultimate periodic solution after the effects of starting the motion have damped out.

Before proceeding with the solution, we comment on a seeming paradox. Physically, it would seem that we could prescribe A in addition to Q because the experimental tube is clamped at its ends over rigid pipes. But the equations admit of only two, not four, boundary conditions. However, the theory does not pretend to take account of the regions at the ends where the area adjusts rapidly to that of the connecting rigid tubes, inasmuch as pressure differences arising from longitudinal curvature and from tube-wall slope have been neglected. The adjustment zone at an end, which zone is actually only a fraction of a tube diameter in length for a thin-walled tube, is excluded from the theory. Thus the areas of the connecting rigid tubes are not relevant. Outside the narrow zone of area adjustment at an end, the area is determined by the pressure according to (6); by using this equation at the end itself, we introduce an error in the adjustment zone, which however has a negligible effect on the solution for the entire tube.

The equations in dimensionless form

To simplify the algebra of the problem we now write the governing equations and their boundary conditions in dimensionless form. The following dimensionless variables are substituted into the governing equations

$$\zeta \equiv A_0/A; \quad v' \equiv v/C_0; \quad C_n' \equiv C_n/C_0; \quad t' \equiv C_0 t/l;$$
$$x' \equiv x/l; \quad \epsilon \equiv Q_0/A_0 C_0; \quad N \equiv \omega l/C_0; \quad F \equiv \tau l/\rho A C_0^2.$$

Equation (1) and (4) then take the dimensionless forms

$$\zeta \partial v/\partial x - v \partial \zeta/\partial x - \partial \zeta/\partial t = 0, \tag{14}$$

$$\partial v/\partial t + v \partial v/\partial x - \zeta \partial \zeta/\partial x + F = 0, \tag{15}$$

where the primes have now been dropped, and it is to be understood henceforth that we are dealing with the normalized forms of all variables.

The quantity F is given as a function of v by one of the three friction relations, (9), (10) or (11). For laminar flow,

$$F = \epsilon S\zeta + v\eta, \tag{16}$$

where $\eta \equiv iN(M_{10}^{-1}e^{-i\epsilon_{10}} - 1)$; $S \equiv \dfrac{isl\mu}{C_0A_0}[8\pi - i\pi\alpha^2(M_{10}^{-1}e^{-i\epsilon_{10}} - 1)]$,

when v and ζ are regarded as complex and the exact relation (9) is used; or where

$$\eta \equiv \frac{N\sin\epsilon_{10}}{M_{10}}; \quad S \equiv \frac{sl\mu}{\rho C_0A_0}\left(8\pi - \pi\alpha^2\frac{\sin\epsilon_{10}}{M_{10}}\right),$$

when v and ζ are regarded as purely real numbers and the approximate relation (10) is used.

For turbulent flow, corresponding to (11),

$$F = \beta\zeta v^{\frac{7}{4}}, \tag{17}$$

where $\beta \equiv 0{\cdot}158(l/D_0)(\mu/\rho C_0D_0)^{\frac{1}{4}}$.

The boundary conditions, (12) and (13), take the normalized forms:

$$\text{at } x = 0: \quad v = \epsilon\zeta(s + \sin Nt), \tag{18}$$

$$\text{at } x = 1: \quad v = \epsilon\zeta s. \tag{19}$$

The linear frictionless solution

Before solving the full problem, it is helpful to get an idea of the form of the solution by dropping the friction terms and considering a motion so small that ζ is almost constant and quadratic terms in v are negligible. The equations then reduce to the classical linear wave equation

$$\partial^2v/\partial x^2 - \partial^2v/\partial t^2 = 0, \tag{20a}$$

which has the general solution

$$v = f(x+t) + g(x-t). \tag{20b}$$

Thus, the dimensionless propagation speed is unity, while, the physical value of C_0 is the propagation speed for frictionless waves of small amplitude.

With the boundary conditions (18) and (19), the solutions are

$$v/\epsilon = s + [\sin N(1-x)](\sin Nt)/\sin N, \tag{21}$$

$$(\zeta - 1)/\epsilon = [\cos N(1-x)](\cos Nt)/\sin N. \tag{22}$$

These represent standing waves which blow up at resonance when N is an integer multiple of π. We can expect that friction will act to suppress the motion at resonance, and that the non-linear effects will distort the waves so that the motions will no longer be sinusoidal in time.

The characteristic equations and their implications

Equations (14) and (15) form a hyperbolic system and, therefore, possess characteristic curves. The equations of the characteristic curves are found by standard methods (Crandall 1956) to be

$$dx/dt = v \pm \zeta \tag{23}$$

for the physical characteristics, which propagate at the physical speed $\pm C_0$ relative to the fluid; and

$$dv = \pm d\zeta - F\,dt \tag{24}$$

for the compatability characteristics.

By considering a frictionless wave of finite amplitude travelling in one direction (a simple wave) we can demonstrate a remarkable property. Suppose it travels to the right. The slope of a right-running characteristic is given by the upper sign in (23): $v+\zeta$. Now, since both v and ζ vary with position on the wave at any instant, we would normally expect the wave to steepen or flatten as it travels down the tube. But this is not so. To determine the relation between v and ζ as we go from one right-running characteristic to the next, we use (24) with the lower sign, which relates v and ζ as we go along a left-running characteristic, and with $F = 0$, from which it is evident that $v+\zeta$ is constant in the simple right-running wave. It follows that every part of the wave moves with the same speed and that the wave neither steepens or flattens.

This extraordinary result depends on the particular pressure-area relation for the tube. For instance, this result cannot be shown when the pressure-area relation derived from Hooke's law is used.† By a combination of non-linear effects, the non-linear stress-strain law leads to a simple result normally associated with purely linear problems.

The exact solution for simple waves without friction

From the fortuitous result above we can anticipate that a solution for frictionless simple waves can be found of the form $f(x \pm t)$, just as in the case of linear waves. This solution is

$$1/\zeta = 1 - f(x \mp t), \tag{25}$$

$$v = \mp \frac{f(x \mp t)}{1 - f(x \mp t)}, \tag{26}$$

where f is any arbitrary function and the $-$ and $+$ signs refer to right- and left-running waves respectively. These solutions may be verified by substitution into (14) and (15), with the friction term omitted.

For right-running waves, v/ζ is the negative of the function f and it is precisely this quantity that is prescribed at $x = 0$ when the tube is driven with a flow

† With the pressure-area relation for Hooke's law, it may be shown that, in a simple wave, a compressive wave steepens for $A/A_n > 16/9$, while a compressive wave broadens for $1 < A/A_n < 16/9$. The converse applies for rarefaction waves. However, the rates of steepening and broadening are very small, much less than in problems of gravity or gas dynamical waves. This is the consequence of the facts that (i) with the pressure-area tube law of (6) there is no change of wave form at all, and (ii) the pressure-area tube law of (6), when graphed, is very close to the pressure-area tube law for a Hookean material.

source. Many other interesting relations between flow, pressure, tube diameter change, etc., can be shown by algebraic manipulation of these simple-wave solutions, and the effects of the non-linear terms can easily be seen.

Perturbation solution with waves of both families

No general solution with waves of both families has been found except for small amplitudes when the linear theory is applicable. Because of the non-linear terms, waves of one family change their speed and amplitude when they pass through waves of the other family. The non-linear theory must be used to describe this behaviour. Yet, because of the particular pressure-area relation for the tube, (6), (7) and (8), a relatively simple perturbation theory is achievable owing to the absence of steepening phenomena associated with each single-wave family.

The parameter ϵ is the appropriate measure of the flow amplitude which controls non-linearities. As ϵ goes to zero, the motion vanishes and the tube area has the undisturbed value, $\zeta = 1$. We therefore expand v and ζ in perturbation series involving integer powers of ϵ:

$$v = \epsilon v_1(x,t) + \epsilon^2 v_2(x,t) + \ldots, \tag{27}$$

$$\zeta - 1 = \epsilon \zeta_1(x,t) + \epsilon^2 \zeta_2(x,t) + \ldots, \tag{28}$$

where the functions $v_1, v_2, \ldots, \zeta_1, \zeta_2, \ldots$ are all assumed to be of order unity. The solutions for these functions are obtained below up to order ϵ^2, thus providing analytical extension beyond the linear theory.

The laminar friction expression with the complex constant relating τ and v, equation (9), is easy to use in the solution for v_1 and ζ_1 because the solution for v_1 is harmonic with frequency N. Since the solution for ζ_2 and v_2 introduces higher harmonics, the friction terms not only become very complicated but the validity of (9) itself becomes questionable. Fortunately, large friction and large ϵ do not occur together either physiologically or in the experiments reported here. We will therefore include friction while solving for v_1 and ζ_1, and neglect it while solving for v_2 and ζ_2. In the worst case calculated, friction represents a 20 % contribution to the solution and non-linearities another 20 %, so that the total error due to neglecting friction in the non-linear terms is 20 % of 20 %, i.e. of the order of 4 %.

We substitute (27) and (28) into (14) and (15), and treat the laminar friction expression as described above. Then, sorting out the respective terms in powers of ϵ, we obtain, for ϵ^1,

$$\partial v_1/\partial x - \partial \zeta_1/\partial t = 0,$$

$$\partial v_1/\partial t - \partial \zeta_1/\partial x + S + v_1 \eta = 0,$$

and for ϵ^2,

$$\partial v_2/\partial x - \partial \zeta_2/\partial t = v_1 \partial \zeta_1/\partial x - \zeta_1 \partial v_1/\partial x,$$

$$\partial v_2/\partial t - \partial \zeta_2/\partial x = \zeta_1 \partial \zeta_1/\partial x - v_1 \partial v_1/\partial x,$$

where the friction terms in the ϵ^2 equations have been dropped and the ϵ^1 solutions appearing in the latter equations are taken to be frictionless. The boundary conditions sorted into powers of ϵ become, for ϵ^1,

$$\text{at } x = 0: \quad v_1 = s + \sin Nt,$$

$$\text{at } x = 1: \quad v_1 = s,$$

and for ϵ^2,

$$\text{at } x = 0\text{: } v_2 = \zeta_1(s + \sin Nt),$$

$$\text{at } x = 1\text{: } v_2 = \zeta_1 s.$$

The ϵ^1 solution is

$$v_1 = \mathrm{Im}\{is + e^{iNt}[\sin N\xi(1-x)]/\sin N\xi\}, \tag{29}$$

$$\zeta_1 = \mathrm{Im}\{i(x-\tfrac{1}{2})T + i\xi e^{iNt}[\cos N\xi(1-x)]/\sin N\xi\}, \tag{30}$$

where

$$\xi \equiv X - iY = M_{10}^{-\frac{1}{2}}[\cos(\tfrac{1}{2}\epsilon_{10}) - i\sin(\tfrac{1}{2}\epsilon_{10})], \tag{31}$$

$$T \equiv 8sN/\alpha^2, \tag{32}$$

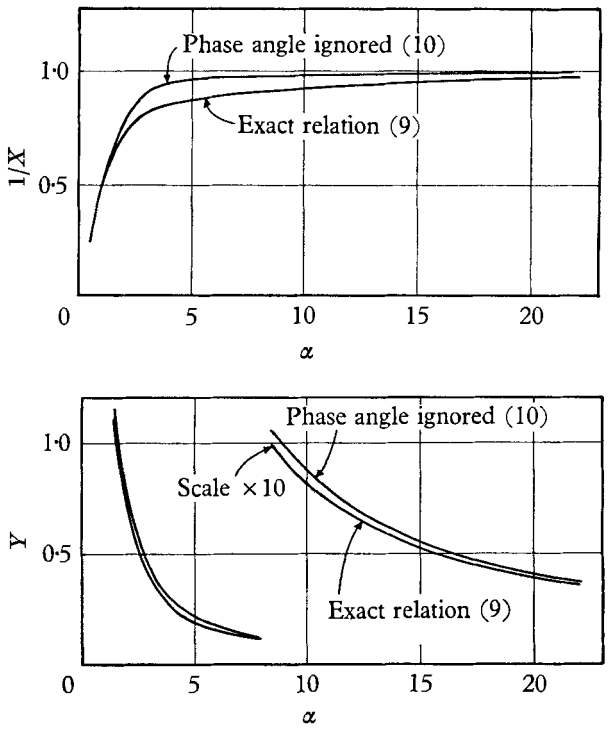

FIGURE 4. The functions $X(\alpha)$ and $Y(\alpha)$, as given by (31).

for the exact laminar friction relation of (9), or

$$\xi \equiv X - iY = \{\tfrac{1}{2}[1 + (M_{10}^{-1}\sin\epsilon_{10})^2]^{\frac{1}{2}} + 1\}^{\frac{1}{2}} - i\{\tfrac{1}{2}[1 + (M_{10}^{-1}\sin\epsilon_{10})^2]^{\frac{1}{2}} - 1\}^{\frac{1}{2}}, \tag{33}$$

for the approximate laminar friction relation of (10). Analysis of (29), (30), (31) and (32) shows that the parameter X modifies the apparent wave speed and produces dispersion, while Y is related to the damping of the waves. Figure 4 shows the values of $1/X$ and of Y as functions of α, both with and without the approximation discussed earlier for the laminar friction in a rigid tube.

The constant of integration $\frac{1}{2}iT$ was evaluated by requiring that at $Nt = \frac{1}{2}\pi$ the tube volume be the same as when $\epsilon = 0$. That is, with the tube driven by a piston, the tube has its original resting volume when the piston is at the centre of its stroke.

When the imaginary part of the solution is taken the final result is

$$v_1 = \frac{fa+gb}{a^2+b^2}\sin Nt + \frac{fb-ga}{a^2+b^2}\cos Nt + s, \tag{34}$$

$$\zeta_1 = \frac{adX-brX+bdY+arY}{a^2+b^2}\cos Nt + (x-\tfrac{1}{2})T + \frac{adY-brY-bdX-arX}{a^2+b^2}\sin Nt, \tag{35}$$

where $a \equiv \sin NX \cosh NY$; $b \equiv \cos NX \sinh NY$;

$d \equiv \cos NX(1-x)\cosh NY(1-x)$; $r = \sin NX(1-x)\sinh NY(1-x)$;

$f \equiv \sin NX(1-x)\cosh NY(1-x)$; $g \equiv \cos NX(1-x)\sinh NY(1-x)$.

By setting $X = 1$ and $Y = 0$, we obtain the frictionless solutions of (21) and (22), which become infinite at resonance. If we consider only a very small amount of friction, so that $X \cong 1$ and $Y \cong 0$, the solutions reduce to forms containing the expression

$$H \equiv \sin N/[\sin^2 N + (NY)^2 \cos N]. \tag{36}$$

Using this, an approximate nearly-frictionless solution for the first-order solutions in v_1 and ζ_1, which has the property of remaining finite at resonance is

$$v_1 = s + H \sin Nt \sin N(1-x), \tag{37}$$

$$\zeta_1 = H \cos Nt \cos N(1-x). \tag{38}$$

This solution is used to evaluate the (v_1, ζ_1) terms appearing in the (v_2, ζ_2) equations.

The solution for the ϵ^2 terms is then

$$v_2 = \frac{H \sin 2Nt}{4}\left[2\cos N(1-2x) - H\sin 2N(1-x) + \frac{\sin 2N(1-x) - \sin 2Nx}{\sin N}\right] + Hs[xN \sin N(1-x) + \cos N(1-x)]\cos Nt, \tag{39}$$

$$\zeta_2 = \tfrac{1}{2}H \sin N + Hs(\sin Nt)[\sin N(1-x) - Nx\cos N(1-x)] - H(\cos Nx)[\sin N(1-x)] + H\sin^2 Nt \sin N(1-2x) + \frac{H\cos 2Nt}{4\sin N}[\cos 2N(1-x) + \cos 2Nx] + H^2 \sin^2 N(1-x)\cos^2 Nt, \tag{40}$$

where the constant $(\frac{1}{2}H)\sin N$ was evaluated by setting the tube volume at $Nt = \frac{1}{2}\pi$ equal to its original resting volume as in the ϵ^1 solution.

This solution in ϵ^2, containing approximations for the friction, should be valid for a laminar flow with any value of α at low ϵ and for laminar flows with large α at higher ϵ. Good accuracy is therefore expected within the physiological range of parameters.

Integration of the characteristics

The numerical integration of the characteristic curves follows conventional methods, in which the solution at a new point is calculated by stepwise integration along the characteristics from the known values of the variables at two earlier

points. We must formulate an initial value problem even though we seek here the steady-state periodic solution which we believe to be independent of transients arising from arbitrary initial conditions. These transients are damped out by viscosity.

The solution is started by choosing initial values for $v(x)$ and $\zeta(x)$ at $t = 0$, as given by the linear solution, (34) and (35). Errors in this initial selection damp out as the computation marches forward in time, and the calculation is continued until the solution is periodic in time. This usually occurs in the time required for a wave to traverse the length of the tube about seven times.

Solutions were obtained with both the turbulent friction relation (11) and the approximate laminar friction relation (10).

5. Experimental apparatus and measurements

The flow source

Figure 5 shows schematically the flow circuit. Except for the elastic tube under test, all piping in the system is rigid. The pumping system is a positive-displacement device in that it produces specified flow wave forms at the tube ends in-

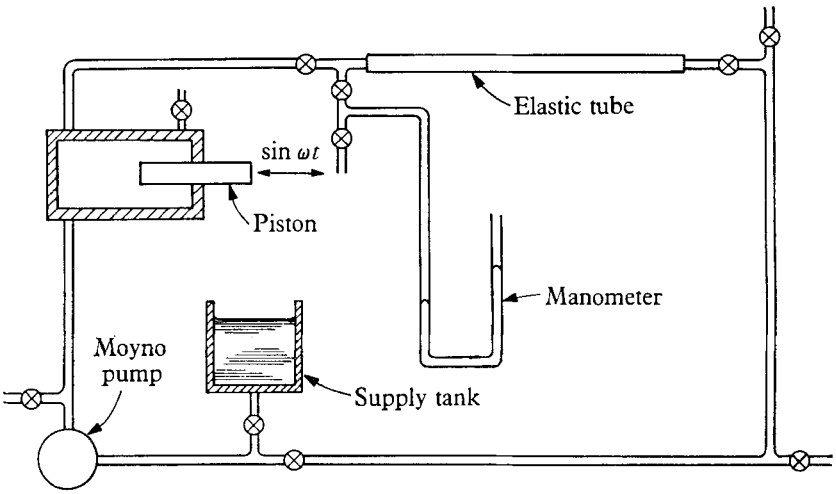

FIGURE 5. Schematic diagram of experimental flow circuit.

dependently of pressure changes. Thus the characteristics of the pumping system do not enter the problem as would be the case if the pump operated by hydrodynamic or peristaltic action. The oscillating and the steady sections of the system are each driven by a $\frac{1}{3}$ hp motor. The total power entering the tube is however less than $\frac{1}{40}$ hp.

A scotch yoke mechanism driving the displacement piston produces at the inlet to the flexible tube a pure sine wave flow containing no higher harmonics. Both the amplitude and frequency of the piston motion are adjustable. Steady flows, free of pulsation, and of any amplitude, are provided by a Moyno positive displacement pump driven through a variable speed drive. The flow at the tube exit is the steady flow component only.

The tube and its properties

The pure latex tubes used, obtained from Kent Latex Products, Inc. of Kent, Ohio, are $\frac{1}{2}$-in. in inside diameter, $\frac{1}{32}$-in. in wall thickness and 35 ft. in length. The relevant constant ρC_n^2 of each tube is measured directly by taking the slope of an experimental pressure-area curve as in figure 1. For the particular tube of figure 1 the value of C_n is 11·23 m/s, with water in the tube.

The tube is constrained longitudinally by cementing it to a rigid table along one edge (figure 6) with a very thin rubber cement in order to achieve as nearly as possible a line contact which, since $\lambda/R \gg 1$, allows nearly axisymmetric radial displacements. The tube is joined to the rigid pipes of the flow system with hose clamps.

The liquid used is either water or, for higher viscosities, a solution of corn syrup in water.

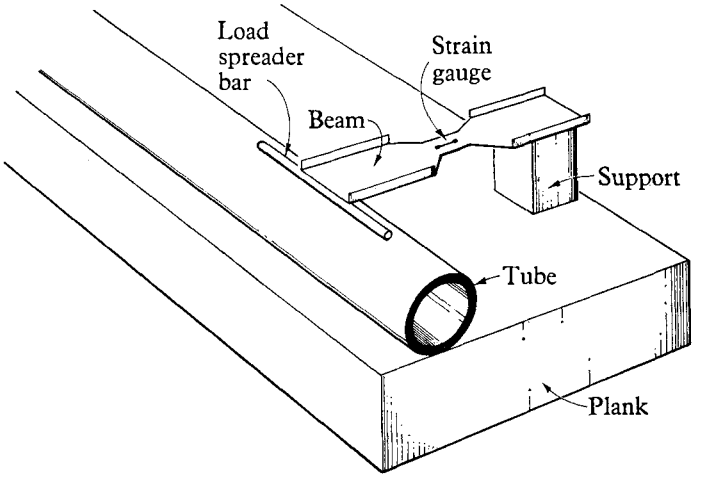

FIGURE 6. Strain-gauge transducer for measurement of external diameter. The elastic tube is cemented to the plank in order to suppress longitudinal strain.

Instrumentation

The outside diameter at ten equally-spaced positions along the tube is measured with strain gauge transducers of the type shown in figure 6. Each transducer has a notch for concentrating the strain in the vicinity of the strain gauges and a small bar for distributing the force over about two diameters of length of the tube. The individual gauges are calibrated by depressing the bar with a dial indicator and adjusting the input voltage until the output is 0·05 volt per inch of deflexion. After this procedure is repeated at each transducer, a known volume of fluid is added to the tube, and the resulting change in reading from each transducer noted. If these readings do not agree with the expected readings to within 2% the tube is rejected as being non-uniform. The sensitivity of the measuring system allows detection of diameter changes of 0·00005 in. In an experimental run the transducers are switched, one at a time, to one channel of a two-channel strip-chart recorder.

The second channel is used to record piston position by means of a transducer comprising a precision potentiometer driven by a gear and rack attached to the scotch yoke mechanism. The signal from this transducer passes through a microswitch tripped by a notch in the driver disk. With the known speed of the chart paper, the distance between spikes gives the period of the motion.

The initial internal pressure in the tube is measured with a mercury manometer, read to $\pm 0{\cdot}1$ mm with a cathetometer.

6. Results

Experimental procedure

An experimental run consists of the following sequence of operations. The tube is inflated to a pressure P_0 while the piston is at rest at the centre of its stroke. This pressure is recorded, and the manometer and supply tank are then shut off from the system. Then the zero points for each of the ten transducers are recorded on the strip-chart recorder. The piston stroke and frequency and the amount of steady flow are set and the flow is started. After a steady state is reached, a few periods of the motion are recorded from each transducer on the strip chart.

Comparison between experimental and theoretical results

The calculation of the theoretical result begins with the experimental values for P_0, piston stroke and frequency, the amount of steady flow, and the fixed parameters of the problem like C_n and the various dimensions of the apparatus. From these values the dimensionless parameters of the theory are calculated and used to predict the motion of the outside of the tube. Since the variable ζ of the theory refers to the inside dimensions of the tube, the theoretical value of the outside diameter is calculated from the theoretical inside diameter by using the assumptions that the volume of the rubber is constant and that there is no longitudinal strain.

The theoretically predicted value of the outside diameter is plotted as a function of time to the same scales as the experimental recording on the strip chart, and the experimental curves are then traced through onto the theoretical plot for comparison. Figure 7 is an example of such a plot.

Each curve in figure 7 shows the outside diameter as a function of time for a fixed position, x, along the tube. The curve at the bottom of the figure is recorded at the tube inlet, $x = 0$. Each higher curve is recorded one tenth of a tube length further down the tube; the top curve is for the far end of the tube, $x = 1$. The line $t = 0$ is shown on the curve taken at $x = 0$ and is in the same horizontal position for the curves at the other values of x. The horizontal line $\Delta D = 0$ is shown at each x-position. This line was not recorded for certain experimental runs so that only the shape, phase, and peak-to-peak amplitude of those runs could be compared with theory. Runs for which the line $\Delta D = 0$ was recorded have a circle about the point $t = 0$, $\Delta D = 0$, as in figure 8. The symbol P, for 'perfect', indicates that the theoretical and experimental curves being compared are virtually coincident.

By producing theoretical curves based on laminar and turbulent friction, respectively, it was found that the turbulent friction approximation more closely

fitted the experimental data whenever the time average of the absolute magnitude of the Reynolds number was greater than about 9500. Accordingly, for Reynolds numbers higher than this, results from the numerical integration of the characteristic curves with the turbulent friction approximation of (11) are presented. For lower Reynolds numbers, the perturbation solution with the laminar friction relation of (9) was used.

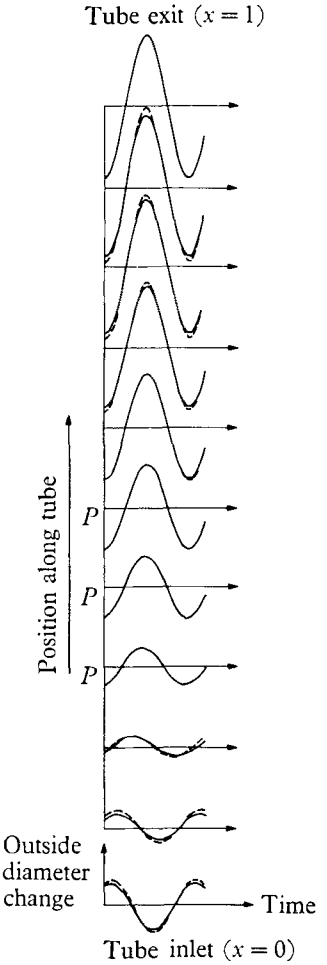

FIGURE 7

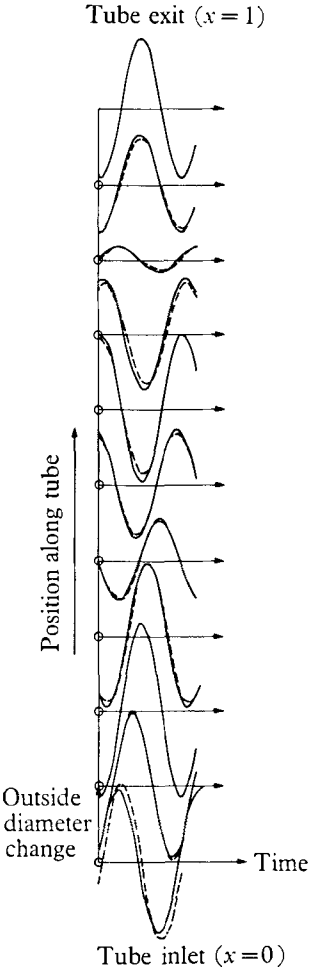

FIGURE 8

FIGURE 7. Comparison of experimental results (dashed) with laminar perturbation theory (solid), for a run (rank 12) in which theory and experiment agree very well, $\epsilon = 0{\cdot}006$, $Re = 947$, $N = 1{\cdot}74$, $s = 0$, $\alpha = 9{\cdot}65$.

FIGURE 8. Rank 23: $\epsilon = 0{\cdot}009$, $Re = 173$, $N = 7{\cdot}36$, $s = 0$, $\alpha = 7{\cdot}22$. Dashed curves: experimental. Solid curves: laminar perturbation theory.

A plot like figure 7 was made for each experimental run and the plots were ranked qualitatively according to degree of agreement between theory and experiment. Table 2 shows the important parameters and degree of agreement for each run. The integers in the column headed 'rank' increase as the agreement

becomes worse. The errors are classified '*A*', '*P*' and '*S*' according to whether the error is mainly one of amplitude, phase, or shape of the curve, respectively.

Sample plots of various ranks are given in figures 7–10.

Effects of the random errors of measurement

Random errors are introduced by inaccuracies in experimental measurements and by the 2 % variations of tube properties. Because of the qualitative nature of the rank rating, variations of ± 5 in rank are not particularly significant. However, the random errors lead to trends that can be seen through this ± 5 scatter in rank.

Consider the effects of errors in N and ϵ on the error in the area change. This error is estimated by differentiating the linear frictionless result of (22):

$$\frac{\Delta(\zeta-1)}{(\zeta-1)_{\max}} = \frac{\Delta\epsilon}{\epsilon} + N\left[(1-x)\sin N(1-x) + \frac{\cos N\cos N(1-x)}{\sin N}\right]\frac{\Delta N}{N}.$$

Errors in area due to errors in N are seen to become important for large N and for values of N near resonance. In fact, for runs with low Reynolds number that are similar except for the value of N (runs 19–22, 47–50, 52–55), the values of rank increase with N within the ± 5 scatter. An exception is run 49 which is near resonance and therefore has a high rank.

Rank	Run	ϵ	Re	N	s	α	Error	Notes
1	21	0·008	1,400	2·325	0	11·56	*A*	—
2	19	0·008	1,200	0·469	0	4·99	*A*	—
3	20	0·008	1,200	1·144	0	7·84	*A*	—
4	38	0·012	262	1·823	0	3·53	*A, P*	—
5	15	0·011	3,100	1·744	0·724	9·65	*A, P*	—
6	37	0·012	256	1·892	0	3·61	*A*	—
7	48	0·009	175	1·321	0	3·04	*A, P*	—
8	8	0·010	1,900	1·627	0	9·27	*A*	—
9	7	0·010	1,800	1·673	0	9·46	*A*	—
10	2	0·011	1,800	1·744	0	9·65	*A*	—
11	3	0·022	3,600	1·744	0	9·65	*A*	—
12	1	0·006	947	1·744	0	9·65	*A*	—
13	47	0·009	179	0·519	0	1·90	*P*	—
14	22	0·009	1,450	6·916	0	19·30	*A, S*	—
15	16	0·011	1,800	1·744	0	9·66	*A*	—
16	6	0·012	1,750	1·815	0	9·89	*A*	—
17	34	0·072	1,440	1·951	0	3·70	*P*	—
18	39	0·011	266	1·765	0	3·45	*A*	—
19	25	0·062	10,300	3·528	0	13·82	*A, S*	—
20	41	0·072	1,620	1·951	0·122	3·69	*A, S*	—
21	53	0·065	1,320	3·811	0	5·18	*A, P*	—
22	9	0·010	1,950	1·577	0	9·10	*A*	—
23	50	0·009	173	7·365	0	7·22	*A, P*	—
24	23	0·061	10,000	0·684	0	6·06	*P*	—
25	31	0·006	125	1·966	0	3·70	*A, P*	—
26	33	0·024	480	1·951	0	3·70	*A, P*	—

(*continued on p.* 533)

TABLE 2. Ranking of experimental runs in order of decreasing agreement with theoretical calculation. The column 'Error' designates whether the discrepancy in the theory is mainly in amplitude (*A*), phase (*P*) or shape (*S*)

By comparing the linear solution of (35) with the frictionless result (22) we see that, as Y goes to zero, the phase angle between the two solutions goes to zero. The phase angle depends on N in addition to Y. Errors in phase angle, therefore, arise from errors in N or Y and are most apparent for large Y. Note that the runs with high α (i.e. low Y) have fewer errors in phase than the runs with low α but with similar values of N (see, for instance, ranks 1 *vs.* 28, 2 *vs.* 13, 3 *vs.* 7, 31 *vs.* 23).

Comparison of laminar and turbulent calculations

When the flow is turbulent rather than laminar, the results are affected in two distinct ways. First, the shear stress at the wall is greater for turbulent flow; and second, the shear stress is not linearly related to the flow. Consequently, the theoretical curves of diameter *vs.* time for turbulent flow differ in amplitude and shape from the corresponding laminar curves. Compare, for instance, figure 9*b* (laminar friction) with figure 9*a* (same data, but turbulent friction). The diameter, and hence pressure, fluctuations at the inlet are greater for the turbulent case; the greater shear stress seems to make it more difficult to drive fluid in and out of the tube. Furthermore, the curve shapes are quite different. This comparison also shows that the theoretical prediction is much improved at this high Reynolds number of 24,800 through the use of the turbulent friction stress.

Rank	Run	ϵ	Re	N	s	α	Error	Notes
27	32	0·013	252	1·961	0	3·70	A, P	—
28	36	0·013	248	2·046	0	3·82	A, P	—
29	52	0·066	1,330	1·518	0	3·27	A, S	—
30	42	0·072	2,580	1·951	0·790	3·69	A, P	—
31	26	0·062	10,200	6·916	0	19·31	A, S	—
32	4	0·066	10,700	1·744	0	9·65	A, S	—
33	44	0·012	428	1·961	0·701	3·70	A, P	—
34	24	0·060	9,800	1·409	0	8·70	S	—
35	45	0·013	1,392	1·951	4·55	3·69	A	*a*
36	5	0·165	24,800	1·731	0	9·65	A, S	*b*
37	11	0·066	19,200	1·744	0·793	9·65	S	*b*
38	10	0·066	28,000	1·735	1·586	9·66	A	*b*
39	54	0·062	1,250	7·436	0	7·25	P	*f*
40	12	0·066	12,200	1·744	0·121	9·65	S	*b*
41	40	0·011	280	1·718	0	3·38	A	—
42	27	0·052	8,500	11·227	0	24·60	A, P	*c*
43	49	0·009	176	2·533	0	4·21	A	*d*
44	14	0·012	10,300	1·744	4·61	9·65	A	*b*
45	43	0·073	3,730	1·966	1·57	3·70	A, S	*e*
46	13	0·012	18,800	1·744	9·21	9·65	A	*b*
47	35	0·138	2,620	1·97	0	3·70	P, S	*g*
48	55	0·062	1,270	13·926	0	9·93	P	*c*
49	46	0·012	2,530	1·966	9·03	3·70	A, S	*e*

Notes: (*a*) A large steady flow can produce a large mean taper in tube, and a small error in the friction can be amplified. (*b*) Turbulent friction assumed in all runs thus marked. (*c*) Large value of N. (*d*) Near resonance. (*e*) Taper incorrect, perhaps because alternately laminar and turbulent. (*f*) Large N, large friction. (*g*) Large ϵ, large friction, perhaps ϵ^2 terms inaccurate in theory.

TABLE 2 (*continued*)

Moreover, the rather good agreement between theory and experiment shown in figure 9*a* suggests that the simple, approximate way of dealing with turbulent friction discussed earlier is adequate for most purposes.

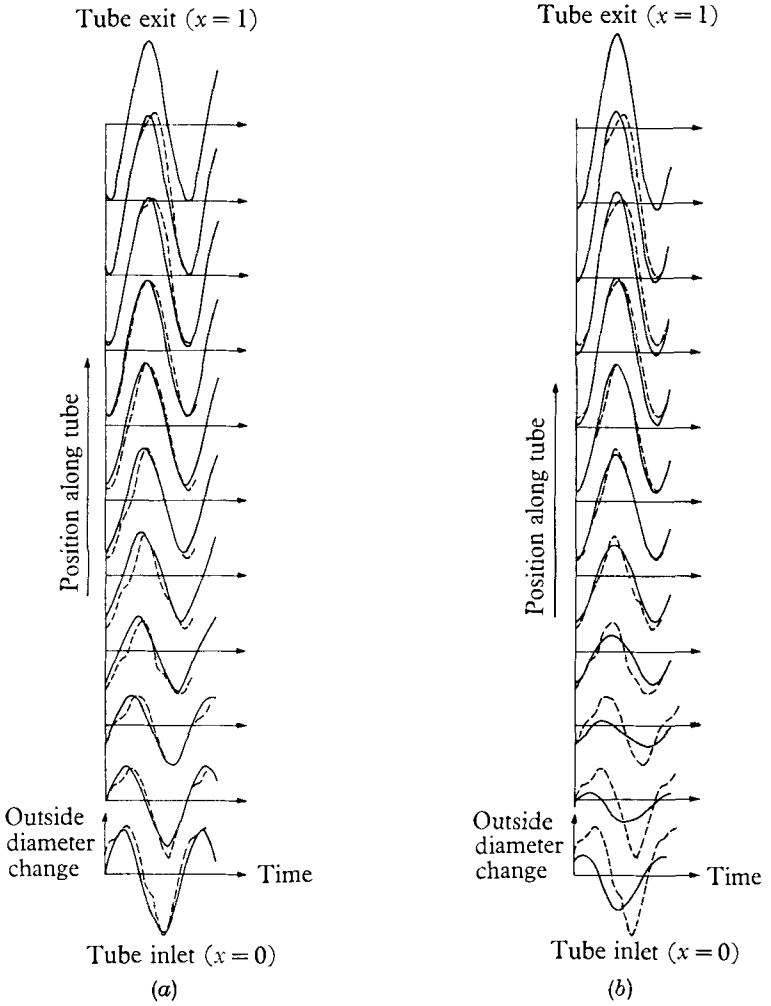

FIGURE 9. Rank 36: $\epsilon = 0{\cdot}165$, $Re = 24{,}800$, $N = 1{\cdot}73$, $s = 0$, $\alpha = 9{\cdot}65$. Dashed curves: experimental. Solid curves: theoretical. (*a*) Characteristics theory, with *turbulent* friction. (*b*) Perturbation theory, with *laminar* friction.

Neither of the theoretical calculations of figures 9*a* and 9*b* exactly match the small irregularities in the experimental curves. The reason is perhaps that the flow is turbulent for only portions of the cycle and that the irregularities result from alternate turbulent and laminar flow in time and space.

Figure 10*b* shows the result of making a calculation for the parameters of figure 10*a* in which the Reynolds number is only 2530, but assuming turbulent rather than laminar flow. In this experimental run, the large amount of steady flow produces a frictional pressure drop and hence a general taper in the tube.

The turbulent calculation (figure 10*b*) predicts an excess taper and the laminar calculation (figure 10*a*) an insufficient taper and, as in figures 9*a* and 9*b*, there are irregularities in the experimental curves. It seems again likely that the flow is not completely laminar or turbulent.

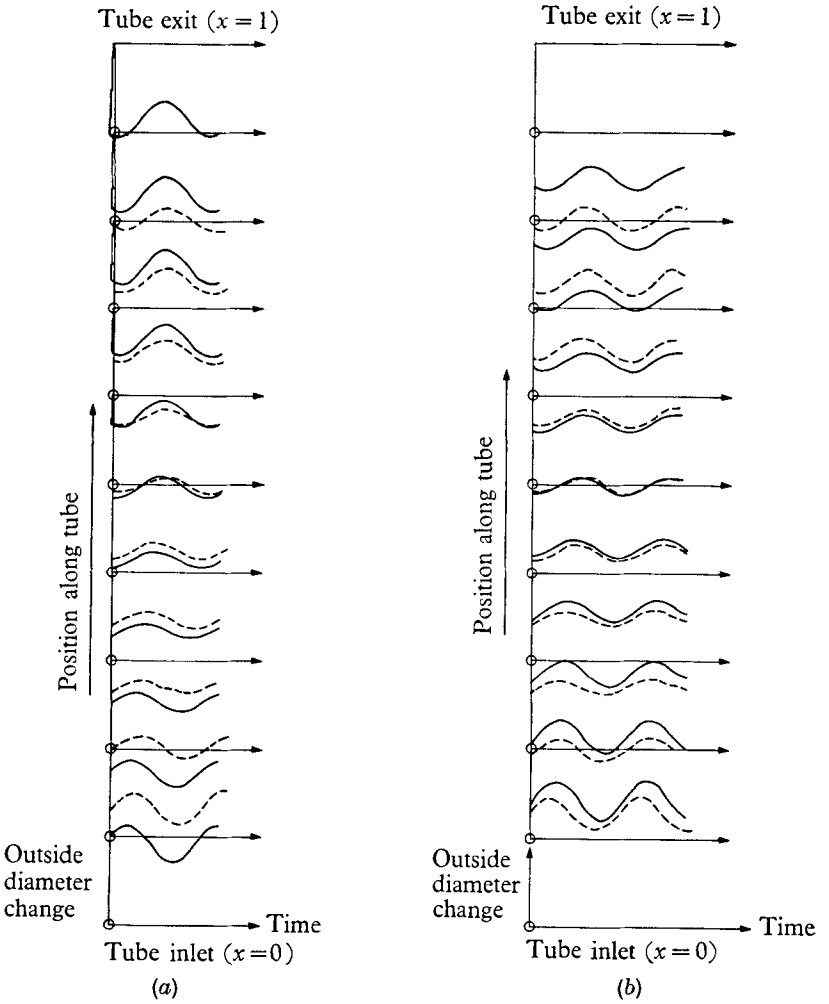

FIGURE 10. Rank 49: $\epsilon = 0{\cdot}012$, $Re = 2530$, $N = 1{\cdot}97$, $s = 9{\cdot}03$, $\alpha = 3{\cdot}70$. Dashed curves: experimental. Solid curves: theoretical. (*a*) Perturbation theory, with *laminar* friction. (*b*) Characteristics theory, with *turbulent* friction.

Figure 11 shows the peak-to-peak diameter fluctuations as a function of x for run 14. Because of the large amount of steady flow, turbulent conditions probably prevail throughout the entire cycle. The node in the motion is seen to be much sharper for the laminar calculation than for both the experimental data and the turbulent calculation. One effect of wall shear stress is to damp the waves; hence, with increased friction, the wave reflected from the far end of the tube is less able to cancel the incident wave at the node. Thus, increased shear stress due to turbulence causes more tube displacement at the nodes.

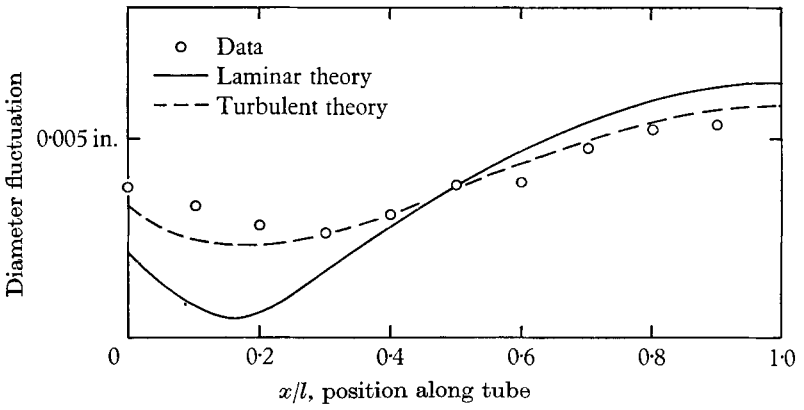

FIGURE 11. Observed peak-to-peak diameter fluctuation as a function of x for run 14, compared with calculations based on laminar and turbulent friction.

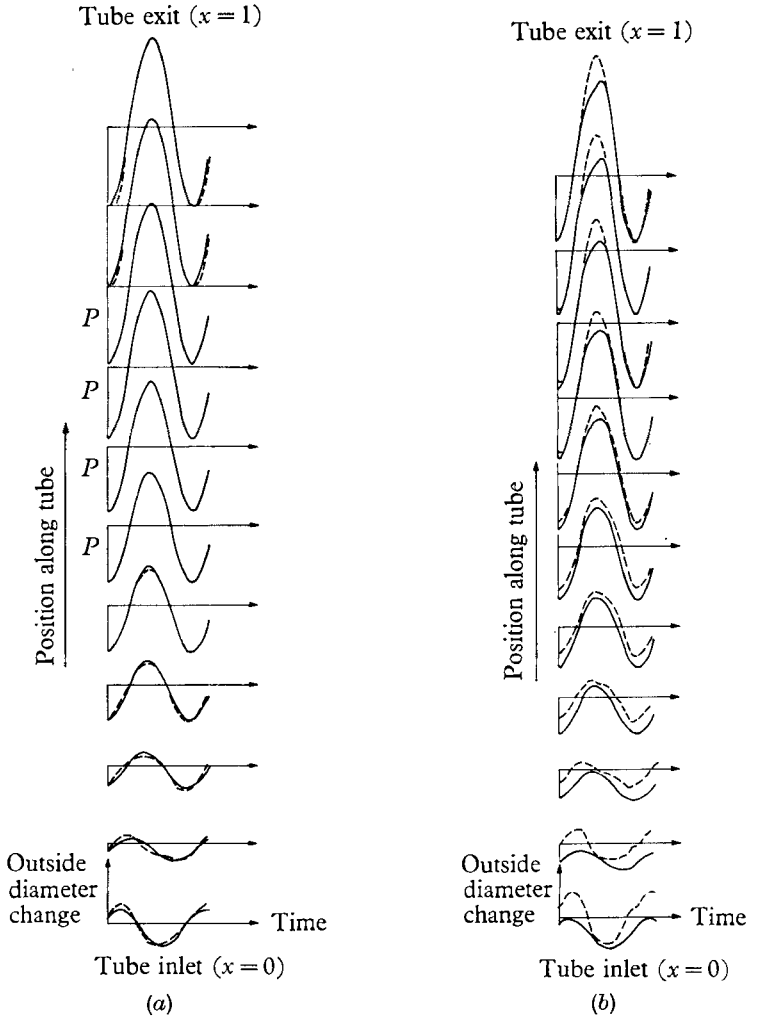

FIGURE 12. Numerical experiment, comparing perturbation theory with characteristics theory, under conditions of small laminar friction (α = 9·65, s = 0, N = 1·73). Dashed curves: characteristics theory. Solid curves: perturbation theory. (*a*) Small amplitude, ϵ = 0·165. (*b*) Large amplitude, ϵ = 0·495.

Range of validity of the perturbation solution

The range of validity for the perturbation solution can be established by numerical experiments in which it is compared with the numerical integration of the characteristics. However, for this comparison the friction expression used in the two solutions must be the same. The approximate laminar friction relation of (10), which is applicable, to both methods, is used.

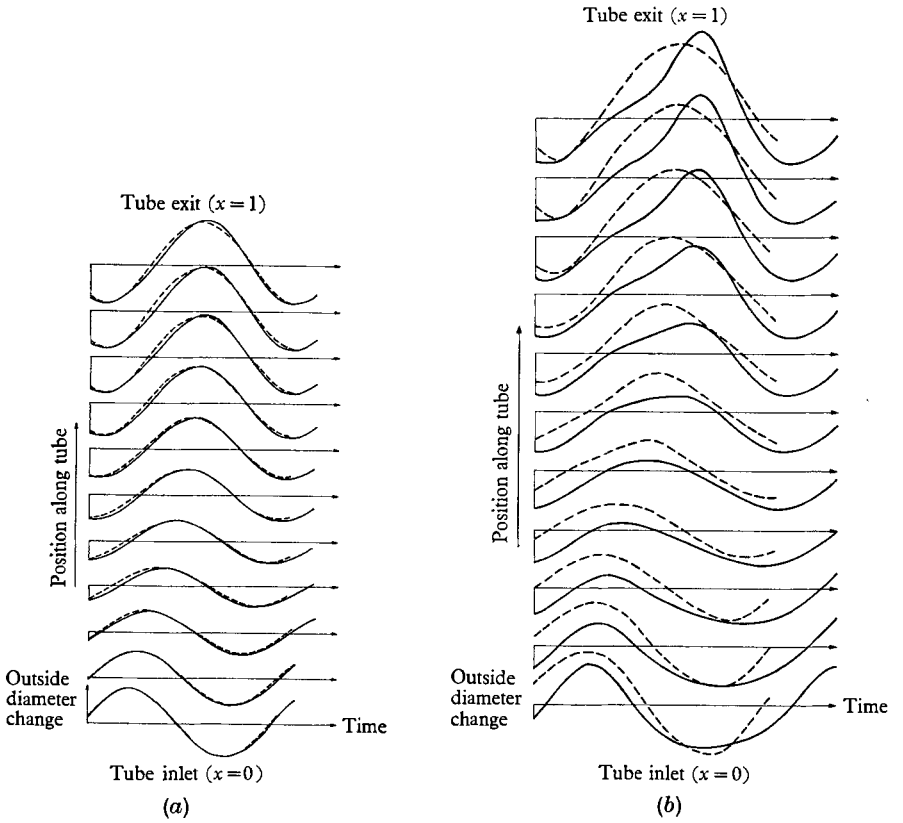

FIGURE 13. Numerical experiment, comparing perturbation theory with characteristics theory, under conditions of large laminar friction ($\alpha = 3{\cdot}70$, $s = 0$, $N = 1{\cdot}97$). Dashed curves: characteristics theory. Solid curves: perturbation theory. (*a*) Small amplitude, $\epsilon = 0{\cdot}138$. (*b*) Large amplitude, $\epsilon = 0{\cdot}415$.

In the perturbation solution friction is neglected in the second-order terms. In the characteristics solution the equations are solved exactly. For this reason the agreement between the two solutions will depend on the values of both ϵ and α. Accordingly, the effects of increases in ϵ were examined, with the other parameters unchanged, for both a low-friction case (run 5) and a high-friction case (run 35).

For values of ϵ less than 0·05, perfect agreement was obtained between the two theoretical methods.

With small laminar friction ($\alpha = 9{\cdot}65$), the comparative results for a three-fold increase in from 0·165 to 0·495 are exhibited in figures 12*a* and 12*b*. A similar

comparison for a three-fold increase in ϵ from 0·138 to 0·415 is shown in figures 13*a* and 13*b* for large laminar friction ($\alpha = 3{\cdot}70$). Significant errors in the perturbation solution appear for values of ϵ as high as 0·4 or 0·5, but the perturbation solution with terms up to ϵ^2 is seen to be adequate for laminar flow within the range of physiological interest as given by the parameters of table 1.

This work was supported in part by grant no. HD01288 from the National Institutes of Health, U.S. Public Health Service, and was also aided by grant no. 647 from the Massachusetts Heart Association and from the Essex North Chapter of the Massachusetts Heart Association.

REFERENCES

CRANDALL, S. H. 1956 *Engineering Analysis*, ch. 6. New York: McGraw-Hill.

LAMBERT, J. W. 1958 On the nonlinearities of fluid flow in rigid tubes. *J. Franklin Inst.* **266**, 83–102.

MORGAN, G. W. & KIELY, J. P. 1954 Wave propagation in a viscous liquid contained in a flexible tube. *JASA* **26**, 323–328.

NICHOLSON, H. 1966 Wave propagation in fluid filled elastic tubes, S.B. Thesis, M.I.T.

OLSEN, J. H. 1966 Waves in fluid-filled elastic tubes. Doctoral Thesis, M.I.T.

ROHSENOW, W. M. & CHOI, H. Y. 1961 *Heat, Mass, and Momentum Transfer*. New Jersey: Prentice-Hall.

RUDINGER, G. 1966 Review of current mathematical methods for the analysis of blood flow. *Proc. Biomed. Fluid Mechs. Symposium, Amer. Soc. of Mech. Engrs, N.Y.*

SCHLICHTING, H. 1960. *Boundary Layer Theory*, p. 299, 4th ed. New York: McGraw-Hill.

STREETER, V. L., KEITZER, W. F. & BOHR, D. F. 1964 Energy dissipation in pulsatile flow through distensible tapered vessels, pp. 149–177, in *Pulsatile Blood Flow*, edited by E. O. Attinger. New York: McGraw-Hill.

TRELOAR, L. R. G. 1958 *The Physics of Rubber Elasticity*, p. 95. Oxford .

WOMERSLEY, J. R. 1957 An elastic tube theory of pulse transmission and oscillatory flow in mammalian arteries. *WADC Tech. Rept.* 56–614.